CORROSION AND TRIBOLOGICAL BEHAVIOR OF ULTRAFINE GRAINED ALUMINIUM ALLOY PROCESSED BY CRYODEFORMATION

[1]Ajith.D, [1]Vinod. B, [1]VinodaKumar Hiremath, [1]Vivek. K, [2]Dasharath S M

[1]Student, [2]Professor
[1]School of Mechanical Engineering
[1]REVA University, Bengaluru, India

Abstract: In the present work, we have reported the corrosion and tribological behavior of Aluminium AL2099 alloy subjected to cryo-rolling under liquid nitrogen temperature [LN_2]. Were the samples are plastically deformed to the obtain reduction in area [RA], i.e. 75%. The mechanical properties of cryorolled samples were investigated by hardness measurement. Enhanced mechanical properties, corrosion and tribological was found in the cryorolled as compared to its coarse grained samples, this is due to grain refinement by the suppression of dynamic recovery and recrystallization during the cryo-rolling.

Keywords: Cryorolling, Ultrafine grains, Corrosion, Wear.

1. Introduction

Age harden-able Aluminium alloys are highly attractive for the excellent mechanical properties such as a high strength-weight ratio, high corrosion resistance, high ductility and strength integrity at low temperatures. These properties have led to its extensive uses in, marine, machinery, aerospace and cryogenic applications [1-3]. There is a great technological interest in bulk ultra-fine grained/nanostructured Al-alloys due to superior mechanical properties [4-6]. Especially, ultra-fine grained 2024 aluminium alloy ('aircraft alloy') emerges as a potential structural material due to its, toughness, high strength and fatigue strength as compared to its conventional grained counterpart [7]. But the preparation of ultra-fine grained bulk Al-alloys is technically very difficult task. Several severe plastic deformation (SPD) techniques are developed to produce bulk ultra-fine grained (UFG) material with homogenized equiaxed grains. The commonly used SPD techniques are High pressure torsion (HPT) [6], Equal channel angular pressing (ECAP) [8], Accumulative roll bonding (ARB) [9], Multi-axial forging (MAF) [7] and cryorolling. But, SPD at room temperature is not very effective to produce ultrafine grained Al-alloys due to the low melting temperatures of the alloys [10]. The suppression of dynamic recovery during deformation at cryogenic temperatures preserves a high density of defects generated by deformation, which can act as the potential recrystallization sites. Accordingly, the cryogenic deformation requires less plastic deformation for achieving UFG structure, compared to the SPD processes [10] at room temperature. Although, theoretically cryorolling is not a SPD process, but it has been identified as one of the advanced processing techniques to develop ultrafine grained structure preferably in the high stacking fault energy (SFE) materials [11] such as Al alloys.

To the best of our knowledge, very few literatures are available on the formation of ultrafine grained 2099 alloy processed by rolling at cryogenic temperature. Hence in the present study, we have investigated the micro-structure, mechanical properties, tribological and corrosion resistance of ultrafine grained Al 2099 alloy processed by cryorolling. The mechanical properties were evaluated by Vickers hardness measurements. The micro-structural evolution was characterized by optical microscope.

2. Methodology

Commercial Al 2099 alloy plates supplied by M/S. Hindalco Industries, India was used the present study. Samples dimensions cut from the plates were 12mm×25mm×32mm, respectively, for cryorolling. The samples were first solution treated (STed) at a temperature 180°C for 10 h in a controlled atmosphere of H_2+argon, and then quenched in the water at room temperature. The samples subjected to cryorolling (Figs.1a show the schematic illustration of cryorolling processes) were well polished along sides to avoid cracking during cryorolling. The STed samples were soaked under liquid nitrogen (LN_2) for sufficient time to achieve LN_2 temperature before each pass till bubbling stops. Rolling was performed through multiple passes and thickness reduction per pass was maintained at 4%. Micro structural characterization was carried out using optical microscopy (Model: Leica DMI 200), Scanning (Model: JEISS51-ADD0048). The microstructural specimens were etched using Poulton reagent. All the samples were prepared in the plane parallel to rolling direction for CR samples. Vickers hardness testing was performed with a load of 1 kg for a dwell time of 10 s. To investigate corrosion resistance of the UFG Al-alloy, potentio-dynamic polarization and tibological tests were carried out for cryorolled samples.

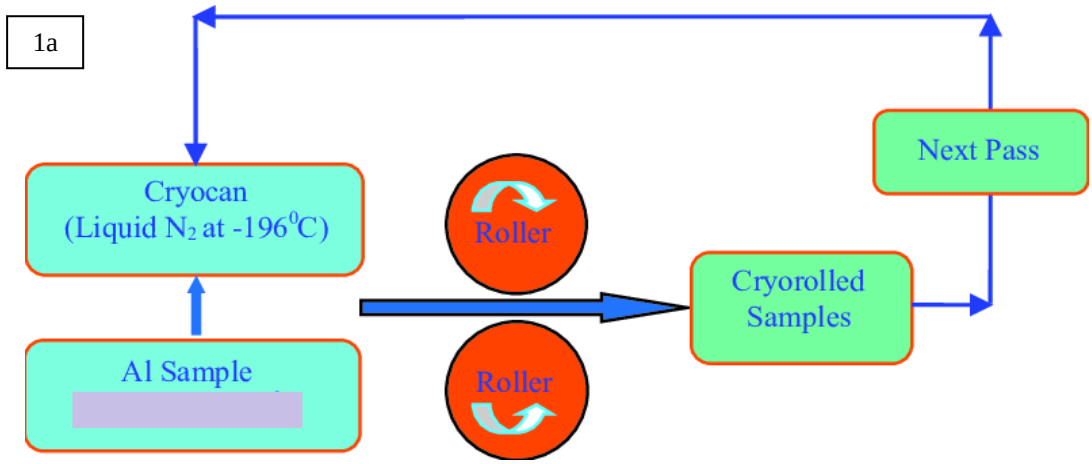

Fig. 1a: Schematic illustration of principle of rolling at liquid nitrogen temperature.

3. Results and discussion

3.1: Microstructure

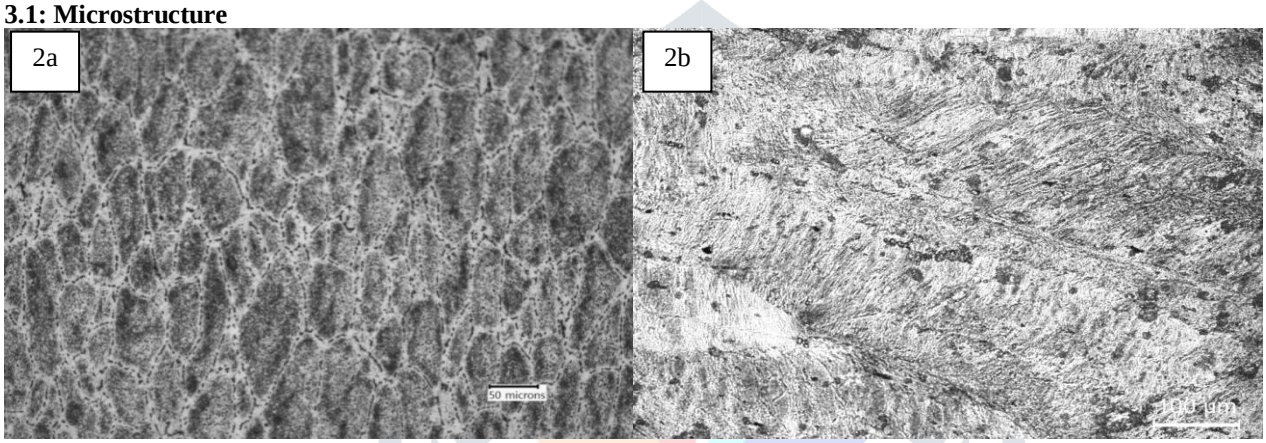

Fig. 2: Optical microstructures of Al 2099 alloy; a) solution treated (STed), (b) CRed.

Fig. 2 shows optical micrographs of the STed cryorolled (CRed samples of Al 2099 alloy. Large size coarse Al alloy grains (~300 µm) can be observed (Fig. 2a) after 10 h of solutionizing followed by quenching in water at room temperature . Appearance of black spots were aligned along with the grain boundaries is supposed to be undissolved second phase precipitates, as also reported in [16]. A bimodal grain structure can observed in the optical micrograph of 75% CRed specimen (Fig. 2b). It can also be noticed that the relatively smaller size elongated grains are observed in comparison to that of the STed sample. Smaller size grains (~50-100 µm) are embedded along with the bigger size (~200-300 µm) grains along the rolling direction. A similar kind of behaviour was reported by Doppalapudi et al. for the CRed samples of Al 2024 alloy [17]. They reported that the STed specimen showed elongated grains size of 300-400 µm, whereas, the CRed (80%) specimen after aging (12 h at 190ºC) showed smaller size recrystallized grains (30-50 µm) embedded along with the bigger size grains (300-400 µm). Rao et al. [7] reported that the average grain size of the STed Al 6061 alloy specimen was ~300 µm, but after MAF (equivalent true strain=5.4) in cryogenic temperature, the grain size reduced to the range of 0.1-0.3 µm. The formation of such finer grains might be due to the accumulation of large amount of deformation strain. Figs. 2c and d, respectively, show the optical images of the 2 ($\Sigma\Delta\varepsilon$=1.2) and 4 cycles ($\Sigma\Delta\varepsilon$=2.4) cryoforged samples. Rolling at cryogenic temperature leads to the formation of deformed microstructure consisting of deformation bands. It will be clearly seen in fig. 2b that with increasing strain the density of deformation bands increased. This is in agreement with the Kobayashi et al. [18]. Under severe plastic deformation at the low temperatures, several geometrically necessary boundaries (GNBs) such as micro bands or deformation bands [19] are easily developed. The mutual crossing, number of deformation bands and misorientation of deformation bands increases with strain; finally resulting in evolution of new fine grains.

3.2: Mechanical properties

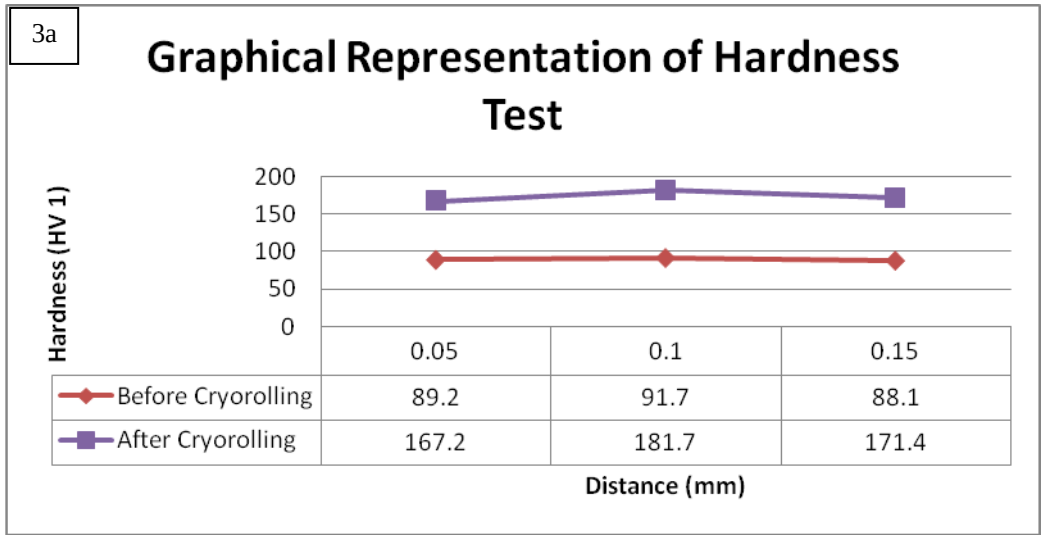

Fig. 3a: Variation of hardness as a function of reduction.

Sample preparation for hardness tests were done on the plane parallel to the rolling direction for the CRed samples. The maximum RA (75%) CRed specimen showed an improved hardness of 181.7 Hv compared to the STed sample of 91.7 Hv, as shown in Fig.3a. This increment in the hardness is purely due to sub grains boundary strengthening, dislocation strengthening, and solid solution strengthening. The increment in the hardness of CRed sample is the combined effect of solid solution strengthening, work hardening and Hall-Patch effect.

3.3: Corrosion test

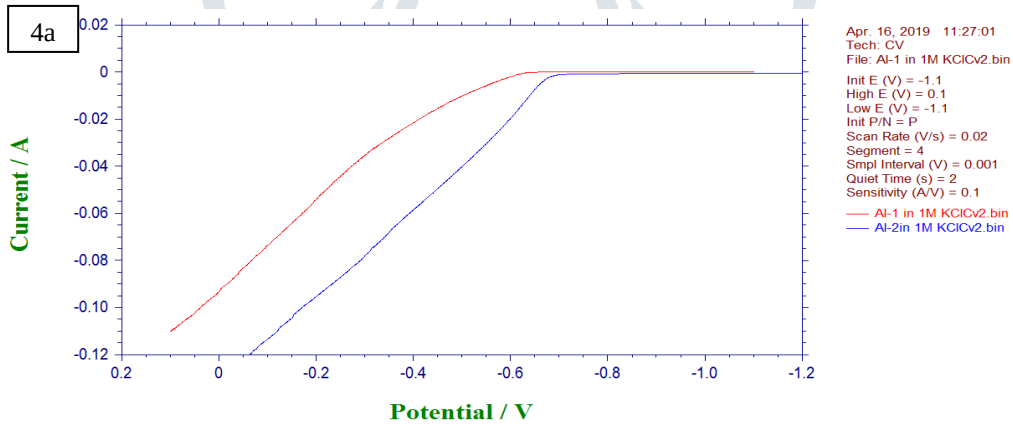

Fig. 4a: Potentiodynamic polarization scans of Al 2099 alloy subjected to before cryorolling and after cryorolling.

Fig. 4a: shows the Potentiodynamic polarization scans of Al 2099 alloy subjected to before cryorolling and after cryorolling. The cryorolled specimen showed relatively a higher corrosion resistance compared to that of unrolled specimens. The progressive depletion of Cu and Li from the matrix due to the formation of strengthening precipitates on the aging increases the resistance to corrosion. Also more grain boundary area of the fine grained structure reduces chloride concentration per grain boundary area resulting in less current density. On the other hand, the homogenized samples show poor corrosion resistance due to enrichment of Cu and Li in the solid solution of the alloy. This decreased the ability to sustain catholic reactions resulting in increase in the susceptibility to corrosion.

3.4. Wear Test

3.4.1. Specifications of Instrument

- Description: PIN/BALL ON DISC TESTER TR 20LE
- Model No: TR 20LE
- Pin Diameter: 3-12 mm
- Ball Diameter: 10 mm
- Disc (Diameter x Thickness): 165 x 8 mm
- Wear track diameter: 50-140 mm
- Sliding Velocity: 0.5-10 m/s
- Disc Speed: 200-2000 rpm
- Normal Load: 5-200 N
- Frictional Force: 0-200 N
- Wear: 0-2000 µm

3.4.2. Testing Procedure

- Cleaned samples are fixed in the chuck of the wear testing machine.
- Select the Wear Track Diameter and Load of the Rotating Disc.
- Select the Speed (200,300,400rpm) to be applied.
- Start the machine.
- Take the Wear readings and Frictional force at equal time intervals.
- Calculate Wear rate and Co-efficient of friction by using suitable formulae.
- Plot the graph of Wear rate v/s Sliding Distance and Co-efficient of friction v/s Sliding Distance.
- Repeat the steps for different materials.

3.4.3. Tabulation and Calculations with Graphical Representation of Wear Test

The following Wear readings and Frictional force for different speed with constant load were observed for the samples:

Table 1: Wear readings and Frictional force

Sl. No.	Samples	Time, min	Wear, µm			Frictional Force, N		
			Speed			Speed		
			200rpm	300rpm	400rpm	200rpm	300rpm	400rpm
1	Before Rolling (Sample 1)	2	9.34	49.33	34.31	2.42	3.79	4.56
		4	18.94	56.00	64.09	2.54	3.25	4.62
		6	33.22	66.96	95.03	2.84	3.29	4.73
		8	45.96	80.94	125.20	3.93	4.16	4.82
		10	58.63	105.78	165.62	3.96	4.35	4.98
2	After Rolling (Sample 2)	2	136.93	17.80	32.38	3.54	2.97	4.92
		4	152.22	46.31	76.25	3.29	4.03	4.67
		6	180.66	68.23	119.91	3.86	4.19	5.02
		8	217.72	102.01	167.17	3.58	4.27	4.60
		10	237.34	134.88	205.24	3.97	4.17	4.62

The data required for the calculations are as follows:

- Length of the specimen = 9mm
- Width of the specimen= 5 mm
- Track radius (R) = 100mm
- Speed of rotating disc (N) = 200 rpm,300 rpm,400rpm

- Normal Load (L) = 10N
- Density of the Specimen = 2.7 x 10^{-3} gm/mm^3

The calculations for the Wear rate and Co-efficient of friction are as follows

- Area of the specimen = l*b in mm^2 =9*5 **= 45mm^2**
- Sliding Distance = (2 π R N x Time in mins) in mm = 2 x π x 100 x 200 x 2
  = 0.251x 10^6 mm
- Co-efficient of friction (μ) = $\frac{\text{Frictional force (F)}}{\text{Normal load (L)}} = \frac{2.42}{10}$ = **0.242**
- Wear rate =

$$\left[\frac{\text{Wear Indicator reading} * \text{Cross sectional area of the specimen} * \text{Density of the specimen}}{\text{Sliding Distance}}\right] * 10^3$$

$\frac{0.00934 * 45 * 0.0027}{251000}$ **= 4.51x $10^{-6}$$mm^3$/s**

3.4.4. Result Tabulation

The calculated values of wear rate and co-efficient of friction for corresponding sliding distance is tabulated.
Sample 1: Before Rolling

Table 2: Wear rate and Co-efficient of Friction

Sl. No.	Speed (N) rpm	Time, min	Sliding Distance, mm	Wear rate, mm3/sec	Coefficient of Friction
				Load	Load
				10N	10N
1	200	2	0.251x 10^6	4.51x 10^{-6}	0.242
		4	0.502x 10^6	4.575x 10^{-6}	0.254
		6	0.753x 10^6	5.35x 10^{-6}	0.284
		8	1.005x10^6	5.55x 10^{-6}	0.393
		10	1.25x10^6	5.69x 10^{-6}	0.396
2	300	2	0.376x10^6	1.589x 10^{-6}	0.379
		4	0.753x10^6	9.02x 10^{-6}	0.325
		6	1.130x10^6	7.19x 10^{-6}	0.329
		8	1.507 x10^6	6.52x 10^{-6}	0.416
		10	1.884x 10^6	6.81x 10^{-6}	0.435
3	400	2	0.502x 10^6	8.29x 10^{-6}	0.456
		4	1.005x 10^6	7.74x 10^{-6}	0.462
		6	1.507x 10^6	7.65x 10^{-6}	0.473
		8	2.01x 10^6	7.56x 10^{-6}	0.482
		10	2.51x 10^6	8.006x 10^{-6}	0.498

Sample 2: After Rolling

Table 3: Wear rate and Co-efficient of Friction

Sl. No.	Speed (N) rpm	Time, min	Sliding Distance mm	Wear rate, mm3/sec	Co-efficient of Friction
				Load	Load
				10N	10N
1	200	2	0.251x 10^6	$2.35x\ 10^{-5}$	0.354
		4	0.502x 10^6	$1.308x\ 10^{-4}$	0.329
		6	0.753x 10^6	$1.035x\ 10^{-4}$	0.386
		8	1.005x 10^6	$9.355x\ 10^{-5}$	0.358
		10	1.25x 10^6	$8.159x\ 10^{-5}$	0.397
2	300	2	0.376x 10^6	$2.03x\ 10^{-6}$	0.297
		4	0.753x 10^6	$2.65x\ 10^{-6}$	0.403
		6	1.130x 10^6	$2.60x\ 10^{-6}$	0.419
		8	1.507x 10^6	$2.92x\ 10^{-6}$	0427
		10	1.884x 10^6	$3.09x\ 10^{-6}$	0.417
3	400	2	0.502x 10^6	$2.78x\ 10^{-6}$	0.492
		4	1.005x 10^6	$3.27x\ 10^{-6}$	0.467
		6	1.507x 10^6	$3.435x\ 10^{-6}$	0.502
		8	2.01x 10^6	$3.59x\ 10^{-6}$	0.460
		10	2.51x 10^6	$3.52x\ 10^{-6}$	0.462

3.4.5. Graphical Representation of Wear Test

The graphical representation of wear rate for corresponding sliding distance.

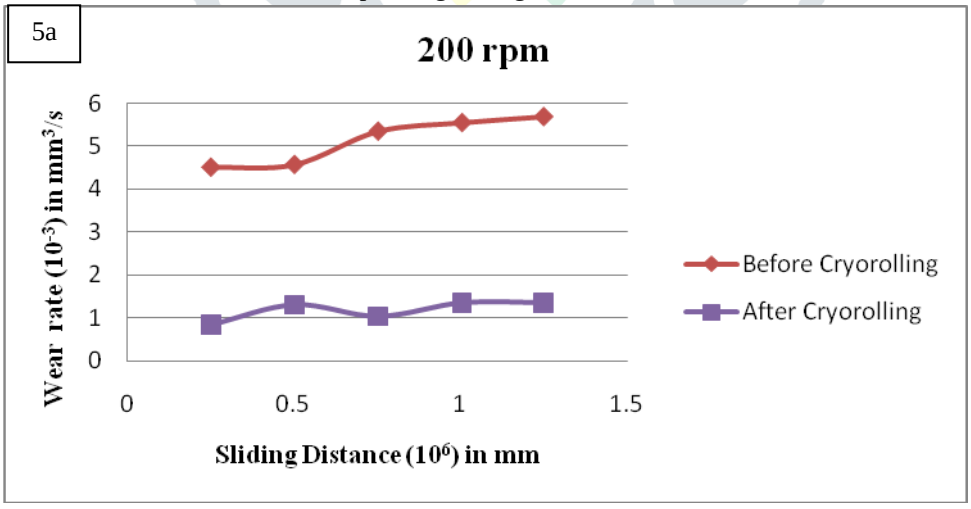

Fig.5 (a):- Graph of Wear rate v/s Sliding Distance for 200rpm

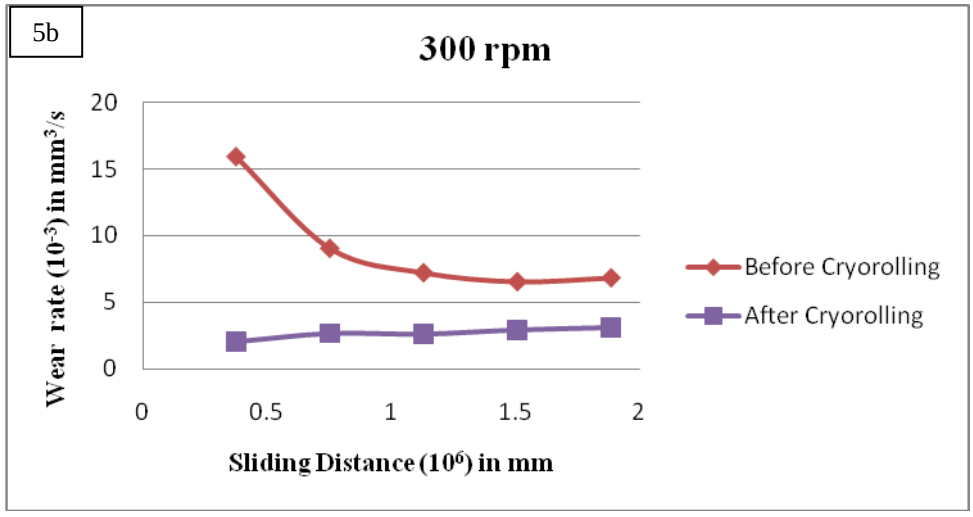

Fig.5 (b):-Graph of Wear rate v/s Sliding Distance for 300rpm

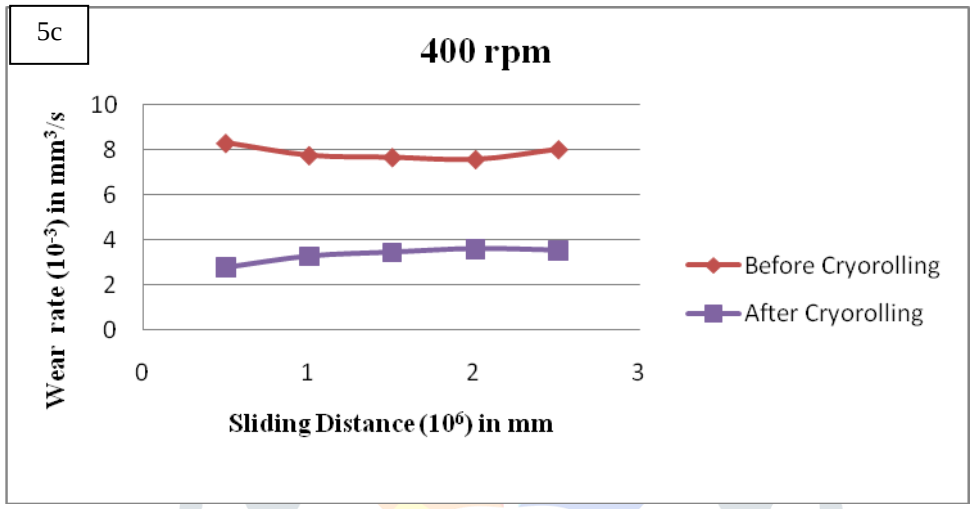

Fig.5(c):- Graph of Wear rate v/s Sliding Distance for 400rpm

The graphical representation of coefficient of friction for corresponding sliding distance

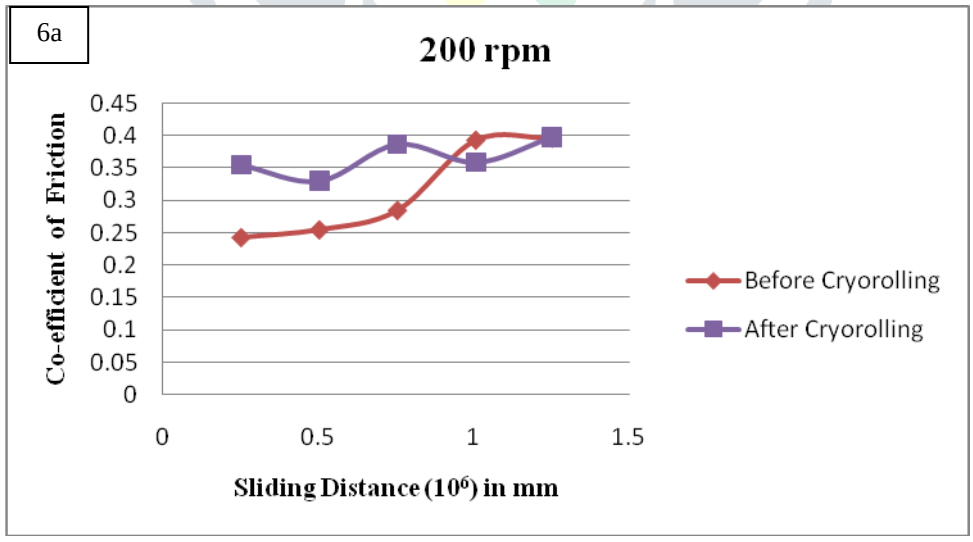

Fig 6(a):- Graph of Co-efficient of friction v/s Sliding Distance for 200rpm

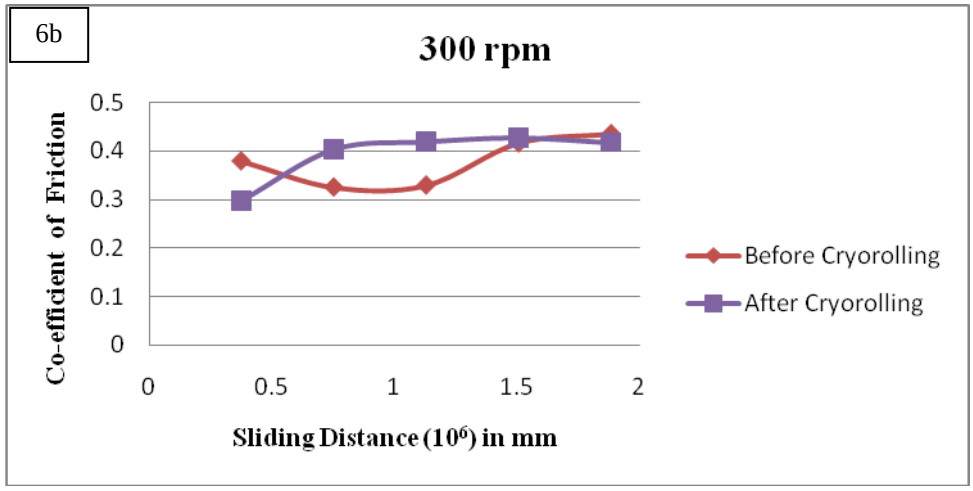

Fig 6(b):-Graph of Co-efficient of friction v/s Sliding Distance for 300rpm

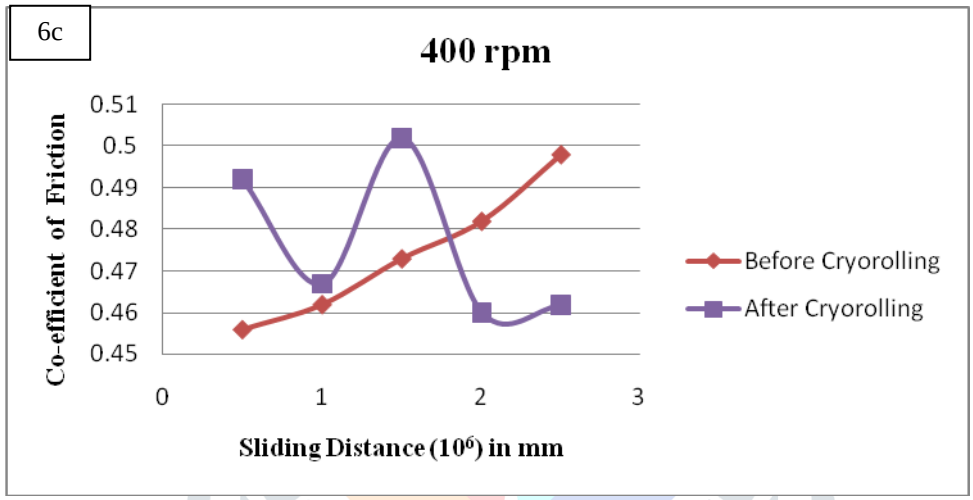

Fig 6(c):- Graph of Co-efficient of friction v/s Sliding Distance for 400rpm

The fig 5a,5b,5c shows the graphical representation of wear rate for corresponding sliding distance for before and after cryorolling samples, we found that the wear rate for after cryorolling samples is less as compared to before cryorolling samples.

The fig 6a,b,c shows the graphical representation of co-efficient of friction for corresponding sliding distance for before and after cryorolling samples , we found that co-efficient of friction of the cryorolled samples is lesser compared to unrolled samples. Where we absorbed that the co-efficient of friction varies with respect to speed. Hence the friction rate is lower that the unrolled samples.

3.5: Conclusions

Cryorolled sample of aluminium AL2099 alloy with 75% RA showed the highest value of mechanical properties (Hardnes-181.7Hv) as compared to that of coarse grain counterpart. This is due to the saturation of dislocation density and refinement of grain size during the cryorolling.

Acknowledgement

We would like to extend our gratitude for Dr. K S Narayanaswamy, Director, School of Mechanical Engineering, REVA University for supporting and encouraging us to carry out this study with required facilities from University.

References

[1] J.W. Evancho,J.G.Kaufmann: New 6XXX-seires alloys for auto body sheet, ALUMINIUM vol. 53, 1977, pp. 609 - 613.

[2] D.G. Altenpohl: Aluminium, technology, applications, and environment, a profile of a modern metal, sixth edition, TMS, 1998, pp. 360–364.

[3] L.P. Troeger and E.A. Starke: Mater. Sci. Eng., 2000, vol. A277, pp. 102-113.

[4] R.Z. Valiev, R.K. Islamgaliev, I.V. Alexandrov: Bulk Nanostructured Materials from Severe Plastic Deformation, Prog. Mater. Sci. 2000, vol. 45, pp. 103–189.

[5] R.Z. Valiev, T.G. Langdon: Principles of ECAP as a processing tool for grain refinement, Prog. Mater. Sci. 2006, vol. 51, pp. 881–981.

[6] A.P. Zhilayev and T.G. Langdon: Using high pressure torsion for metal processing, Progress in Mater. Sci. 2008, vol. 53, pp. 893–979.

[7] P.N. Rao, D. Singh, R. Jayaganthan: Mechanical properties and microstructural evolution of Al 6061 alloy processed by MAF at LN2 temp.", Mater. and Design, 2014,vol.56, pp. 97–104.

[8] Y.H. Zhao, X.Z. Liao, Z. Jin, R.Z. Valiev, Y.T. Zhu: Microstructures and mechanical properties of UFG 7075 Al alloy processed by ECAP and their evolutions during annealing, Acta Materialia, 2004, vol. 52, pp. 4589–4599.

[9] M. Eizadjou, H.D. Manesh, K. Janghorban: Microstructure and mechanical properties of UFG Al strips produced by ARB process, Journal of Alloys and Compounds, 2009, vol. 474, pp. 406–415.

[10] Y. Wang, M. Chen, F. Zhou and E Ma: High tensile ductility in a nanostructured metal, Nature, 2002, vol. 419, pp.912-915.

[11] V.S. Sarma, J.Wang , W.W. Jian , A. Kauffmann , H. Conrad, J. Freudenberger: Role of stacking fault energy in strengthening due to cryodeformation of FCC metals, Mater. Sci., 2010, vol. 527, pp. 7624–7630.

[12] Y. SAITO, N. TSUJI, H. UTSUNOMIYA, T. SAKAI AND R.G. HONG: ULTRA-FINE GRAINED BULK ALUMINUM PRODUCED BY ACCUMULATIVE ROLL-BONDING (ARB) PROCESS, SCR. MATER, 1998, VOL. 39, PP. 1221-1227.

[13] Y.H. Zhao, X.Z. Liao, S. Cheng, E. Ma and Y.T. Zhu: Simultaneously Increasing the Ductility and Strength of Nanostructured Alloys, Adv. Mater., 2006, vol. 18, pp. 2280.

[14] G. Sevillano and Aldazabal: Ductilization of nanocrystalline materials for structural applications, Scripta Materialia, 2008, vol. 51, pp. 795−800.

[15] D.G. Atlenpohl: Corrosion Resistance and Protection, Aluminum Technology, Applications, and Environment [M], 6th ed. Warendale, TMS, 1998, p. 29.

[16] G. Das, M. Das, S. Ghosh, P. Dubey, A.K. Ray: Effect of aging on mechanical properties of 6063 Al-alloy using instrumented ball indentation technique, Materials Science and Engineering A, 2010, vol. 527, pp. 1590-1594.

[17] D. Doppalapudi, P. Venkatachalam, S. Ramesh Kumar, B. Ravisankar, K. Jayashankar: Improving the mechanical properties of 2024 Al alloy by cryo rolling, TIIM, 2010, vol. 63, pp. 31-34.

[18] C. Kobayashi, T. Sakai, A Belyakov, H Miura: Ultrafine grain development in copper during multidirectional forging at 195 K, Philos. Mag. Lett., 2007, vol. 87, pp. 751-66.